iScience

CellPress
OPEN ACCESS

Article

Kynurenine Metabolism in the Fat Body Non-autonomously Regulates Imaginal Disc Repair in *Drosophila*

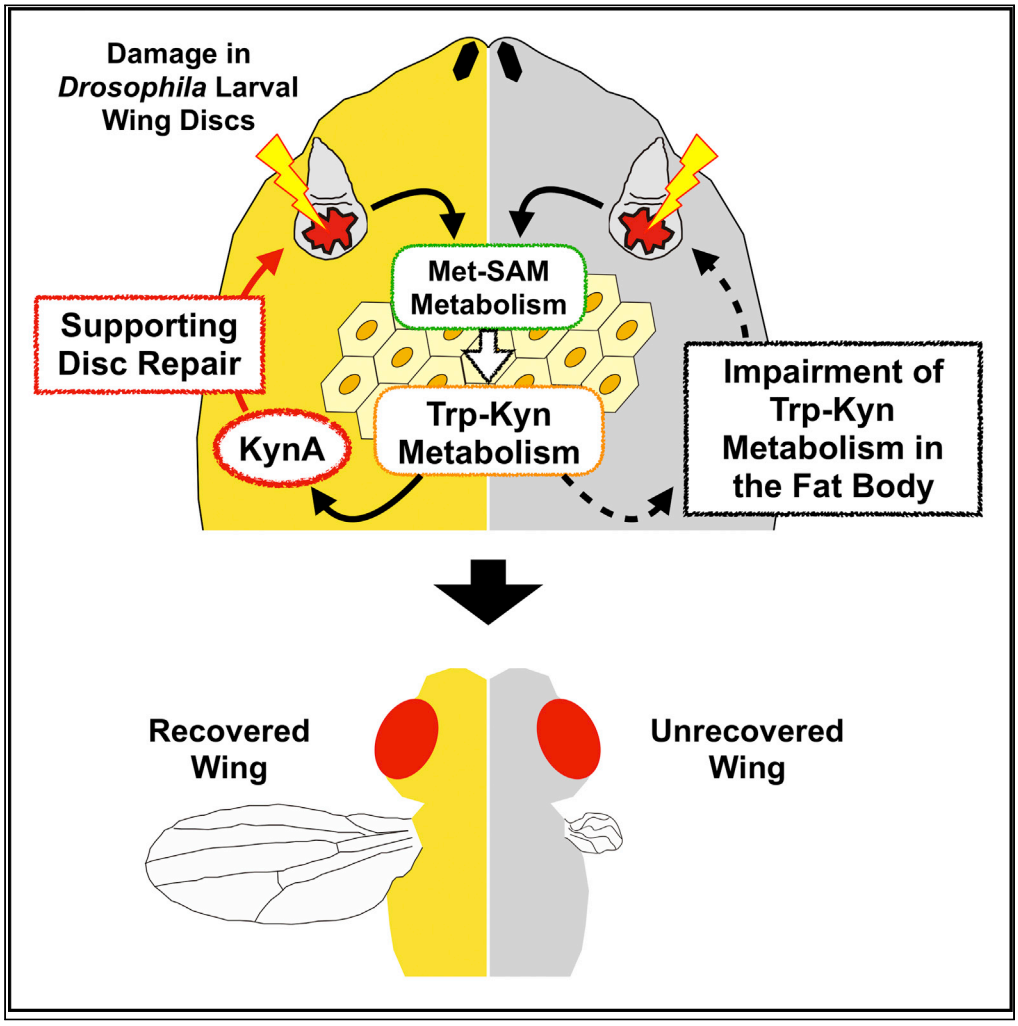

Soshiro Kashio,
Masayuki Miura

miura@mol.f.u-tokyo.ac.jp

HIGHLIGHTS

Trp-Kyn pathway in *Drosophila* larval fat body is remotely required for disc repair

The fat body-derived humoral KynA is required for disc repair

SAM synthesis in the fat body affects KynA levels in hemolymph during disc repair

Kashio & Miura, iScience *23*, 101738
December 18, 2020
https://doi.org/10.1016/j.isci.2020.101738

iScience

CellPress
OPEN ACCESS

Article

Kynurenine Metabolism in the Fat Body Non-autonomously Regulates Imaginal Disc Repair in *Drosophila*

Soshiro Kashio[1] and Masayuki Miura[1,2,*]

SUMMARY

Tissue interactions are critical for maintaining homeostasis; however, little is known about how remote tissue regulates regeneration. Previously, we established a genetic dual system that induces cell ablation in *Drosophila* larval imaginal discs and simultaneously manipulates genes in non-damaged tissues. Using humoral metabolome analysis and a genetic damage system, we found that the Tryptophan (Trp)-Kynurenine (Kyn) pathway in the fat body is required for disc repair. Genetic manipulation of Trp-Kyn metabolism in the fat body impaired disc regeneration without affecting wing development. In particular, the fat body-derived humoral kynurenic acid (KynA) was required for disc repair. The impairment of S-adenosylmethionine (SAM) synthesis from methionine (Met) in the fat body hampers the maintenance of KynA levels in hemolymph at the early stage of disc repair, suggesting a connection between Met-SAM and Trp-Kyn metabolisms. Our data indicate KynA from the fat body acts as a permissive metabolite for tissue repair and regeneration.

INTRODUCTION

Tryptophan-kynurenine (Trp-Kyn) metabolites have shown colorful traits in various physiological functions throughout evolution. Trp is an essential amino acid, which serves as a substrate for protein synthesis as well as several bioactive compounds, such as serotonin and melatonin. However, in mammals, the vast majority of the catabolism of Trp happens through the Trp-Kyn pathway and generates a range of metabolites involved in inflammation, immune response, host-microbiome signaling, and neuronal excitability (Cervenka et al., 2017). Kyn is converted into two metabolites, 3-hydroxykynurenine (3-HK) and kynurenic acid (KynA). The metabolite 3-HK is known to exert neural toxicity effects linked to excitotoxicity (Zwilling et al., 2011). Additionally, 3-HK is finally converted to nicotinamide adenine dinucleotide (NAD^+) via quinolinic acid in mammals, although 3-hydroxyanthranilic acid oxygenase or quinolinate phosphoribosyltransferase are not found in *C. elegans* or *Drosophila melanogaster*. On the other hand, KynA shows neuronal protection effects as an antagonist of N-methyl-D-aspartate receptor (NMDAR) and α-7 nicotinic acetylcholine receptor (α7nAChR) (Wirthgen et al., 2018). In addition to such neuronal contributions, Kyn and KynA bind to the transcription factor aryl hydrocarbon receptor (AhR) in immune cells and ameliorate immune activation (Wirthgen et al., 2018). KynA is also reported to bind to orphan G protein-coupled receptor 35 (GPR35) in the intestine and macrophages to modulate mucosal homeostasis or TNF-α secretion (Stone et al., 2013). Thus, the modulation of Trp-Kyn metabolism underlies the mechanisms of diseases.

Tissue damage causes several risks, including infection, tissue malfunction, and even lethality. Multicellular organisms have a homeostatic capacity against tissue damage. However, the underlying mechanisms are not confined to the damaged tissues; rather, they involve organismal regulation, including the immune, nervous, and endocrine systems, and even adipose tissues. Interesting examples of tissue interactions between damaged tissue and other tissues have been reported. When the leg of a mouse is locally injured, the contralateral leg muscle shows a high capacity to reenter the cell cycle in muscle stem cells (MuSCs) through the circulation of hepatocyte growth factor activator (HGFA) (Rodgers et al., 2017). A similar phenomenon is observed in appendage regeneration in axolotls. During blastema formation in a cut appendage, the contralateral uninjured appendage also shows cell proliferation via mTOR signaling (Johnson et al., 2018). We are focusing on such systemic damage responses (SDRs), including systemic wound responses (SWRs) (Kashio et al., 2017). When wounding by simple pricking was performed in adult

[1]Department of Genetics, Graduate School of Pharmaceutical Sciences, The University of Tokyo, 7-3-1 Hongo, Bunkyo-ku, Tokyo 113-0033, Japan

[2]Lead Contact

*Correspondence: miura@mol.f.u-tokyo.ac.jp

https://doi.org/10.1016/j.isci.2020.101738

Drosophila cuticle, an inter-tissue reaction was observed in the intestine and neurons, which are necessary for host survival (Lee and Miura, 2014). Interestingly, SDR also directly contributes to tissue repair processes. For example, reactive oxygen species (ROS) resulting from injuries induce the recruitment of leukocytes (white blood cells), which support fin repair in zebrafish (Yoo et al., 2011).

Despite many advances in the understanding of tissue regeneration, the molecular mechanisms of tissue non-autonomous regulation of repair processes are only beginning to be understood. This could be greatly enhanced by tissue-specific and comprehensive genetic analyses. Previously, we established a genetic cell ablation system for studying non-autonomous aspects of tissue repair in *Drosophila* (Kashio et al., 2016, 2017). *Drosophila* larvae possesses regenerative tissues, imaginal discs, which are known to show a remarkable ability to repair massive tissue damage with surgical ablation or genetic temporal ablation (Worley et al., 2012; Fox et al., 2020). In particular, wing discs are useful to investigate the extent of repair by observing adult wing phenotype. By combining a genetic temporal cell ablation system in imaginal discs with a genetic manipulation system in non-damaged tissues, we can perform functional analyses of systemic aspects of tissue repair. *Drosophila* has tissue-specific gene manipulation systems, such as the Gal4/UAS system and the Q system (Riabinina et al., 2015). We established a cell ablation system using a temperature-sensitive form of the diphtheria toxin A domain (DtA^{ts}) (Bellen et al., 1992). It has been demonstrated that DtA^{ts} is active at low temperatures (18°C) and induces cell death through nuclease activity but is inactivated at high temperatures (29°C) (Lee et al., 2005). Inducing DtA^{ts} expression using the Q system enabled us to manipulate Gal4/UAS-mediated gene expression in other organs, independent of the temporal tissue damage in wing discs. With this genetic "dual" system, we identified that Trp-Kyn metabolism in the fat body, an insect organ that is a functional counterpart of mammalian liver and adipose tissue, is required for disc regeneration without affecting normal wing development. In this study, we found that KynA, an end product of the Trp-Kyn metabolic pathway, is an essential hemolymph metabolite for non-autonomous tissue repair.

RESULTS

Humoral Metabolomic Analysis Reveals that Trp-Kyn Metabolism Is Required for Disc Repair

First, we focused on the hemolymph as an important mediator. Hemolymph has been recognized as a homeostatic regulator at the systemic level (Droujinine and Perrimon, 2016; Leopold and Perrimon, 2007). We collected hemolymph from control and wing disc-damaged larvae at the early stage of disc repair (6 h after cell ablation; AA6) and performed metabolome analysis using capillary electrophoresis time-of-flight mass spectrometry (CE-TOF-MS) to explore the metabolic changes for tissue repair (Figure S1). Our previous data indicated that the levels of one of the essential amino acids, methionine (Met), and its downstream metabolite, S-adenosyl methionine (SAM), were lower in the ablated larval hemolymph at AA6 (Kashio et al., 2016). As expected, the level of Met was lower in disc-ablated larval hemolymph, which verified the metabolome analysis (Figure S1).

The metabolite with the lowest level was Met, whereas tryptophan (Trp) was the metabolite with the highest level in disc-damaged larval hemolymph (Figure S1). *Drosophila* has one rate-limiting enzyme in the Trp-Kyn pathway, Vermilion (V), which is a mammalian ortholog of Tryptophan 2,3-dioxygenase (TDO) (Figure 1A). Similarly to the strong expression of TDO in the mammalian liver (database from The Universal Protein Resource [UniProt]), *vermilion* is predominantly expressed in larval fat body (FB), a counterpart of the mammalian liver and white adipose tissue (data from FlyBase). Therefore, we checked the expression level of *vermilion* in the FB using quantitative RT-PCR (qRT-PCR) at 0 and 6 h after ablation (AA0, 6), and *vermilion* maintained its expression level in the FB of damaged larvae at AA6 (Figures 1A and 1B).

We measured the metabolites of Trp-Kyn metabolism at AA0 and 6 in both disc-damaged and non-damaged larval hemolymph and tissues, including the FB, gut, cuticle (including larval muscle), and brain (Figures S2A–S2E). The level of Trp was higher in disc-damaged larval hemolymph at AA6 (Figure S2A), as observed in metabolome analysis (Figure S1). As for Kyn, the level tended to be higher in damaged larval hemolymph (Figure S2A), which was similar to the level in the FB (Figure S2B) and cuticle at AA0 (Figure S2D). KynA level was higher in almost all samples at AA6 other than brain (Figure S2E).

We also investigated metabolic change during the third larval development. The level of Trp-Kyn metabolites decreased at a whole-body level from the early to late third larval stage (Figure S2F), implying that the

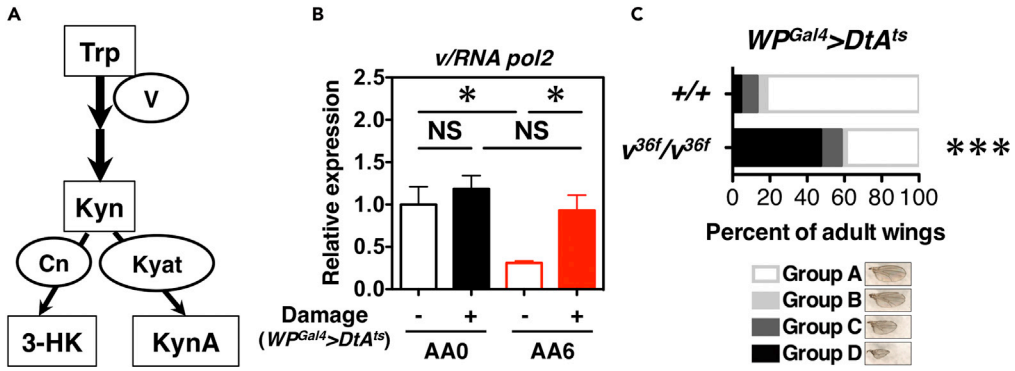

Figure 1. Involvement of Vermilion in Disc Repair

(A) Simplified diagram of Trp-Kyn metabolism. Kyn, Kynurenine; 3-HK, 3-hydroxykynurenine; KynA, Kynurenic acid; V, Vermilion; Cn, Cinnabar; Kyat, Kynurenine aminotransferase.

(B) Expression of *v* in the fat body. Control: +/*UAS-DtA*^{ts}; Ablation: *WP-Gal4/UAS-DtA*^{ts}. SEM was calculated from four independent samples. One-way ANOVA Tukey's multiple comparison test was applied: NS, not significant; *p < 0.05.

(C) *Vermilion* mutant background caused severe wing phenotype after ablation. Statistical analysis was conducted using the Chi-squared test to compare the control (+/+;;*WP*^{Gal4}>*DtA*^{ts}) with *v* mutant (*v*^{36f}/*v*^{36f};;*WP*^{Gal4}>*DtA*^{ts}); ***p < 0.001. Temperature treatment was described in Materials and Methods.

Trp-Kyn metabolism decreased toward the pupation stage and may be correlated with the decrement of the regenerative capacity of the imaginal disc as development proceeds.

FB-Specific Knockdown of *Vermilion* Affects Disc Repair Non-autonomously

To confirm the involvement of Vermilion in disc repair, we performed DtA^{ts} cell ablation with a *vermilion* mutant and it showed a severe wing phenotype (Figure 1C). Previously, oral administration of TDO inhibitor 680C91 was utilized for repressing Vermilion in *Drosophila* and ameliorated neurodegeneration (Breda et al., 2016). Oral administration of 100 μM TDO inhibitor was performed from 24 h before AA6, which resulted in the impairment of disc repair (Figures S3A and S3B). Additionally, TDO inhibitor caused a decrease of the levels of downstream metabolites, 3-HK and KynA (Figure S3C). These results support the contribution of Trp-Kyn metabolism to disc repair.

To investigate the tissue-specific involvement of Vermilion in the FB in disc repair, *vermilion (v)* was knockdown in the FB. Knockdown of *vermilion* did not affect normal wing development but worsened the adult wing phenotype after disc ablation (Figures 2A, 2F, 2G and S5A). We then examined the expression of morphogen Wingless (Wg) and proliferative cells marked with phospho-histone 3 (PH3). At AA0 (following 38 h of cell ablation treatment), there were no significant differences between the control larval discs and *vermilion* knockdown larval discs (Figures 2B, 2C, and 2H). Damaged discs showed a weakened signal of Wg in the wing pouch (WP) region, and the number of PH3-positive cells in the WP region was lower compared with other disc regions. Thirty hours after the shift back to 29°C (condition for cell ablation stop; AA30), cells in the WP were proliferating and the typical Wg staining pattern was restored during the recovery phase in control discs (Figures 2D, 2D′, and 2H), indicating that the repair process had been activated. On the other hand, wing discs in FB-specific *vermilion* knockdown larvae indicated a hampered repatterning of Wg without substantial differences in cell proliferation (Figures 2E, 2 E′, and 2H). Additionally, the knockdown of *vermilion* in the WP region did not worsen wing normal development and disc repair (Figure S3D, S5C and S5D), which supports the idea that Vermilion acts non-autonomously in disc repair.

Previous studies indicated that damage in discs causes a developmental delay, which is required for modulating organ size control (Colombani et al., 2012; Garelli et al., 2012; Halme et al., 2010). The influence of Vermilion on developmental timing was not observed in either damaged or non-damaged conditions (Figure 2I), indicating that Vermilion regulates disc repair by affecting the repair processes and not the developmental timing.

We also examined tissue remodeling and dying cell clearance with phalloidin (F-actin probe) and active executioner caspase, Dcp1, antibody staining. Recent studies indicated that dying cell clearance and tissue

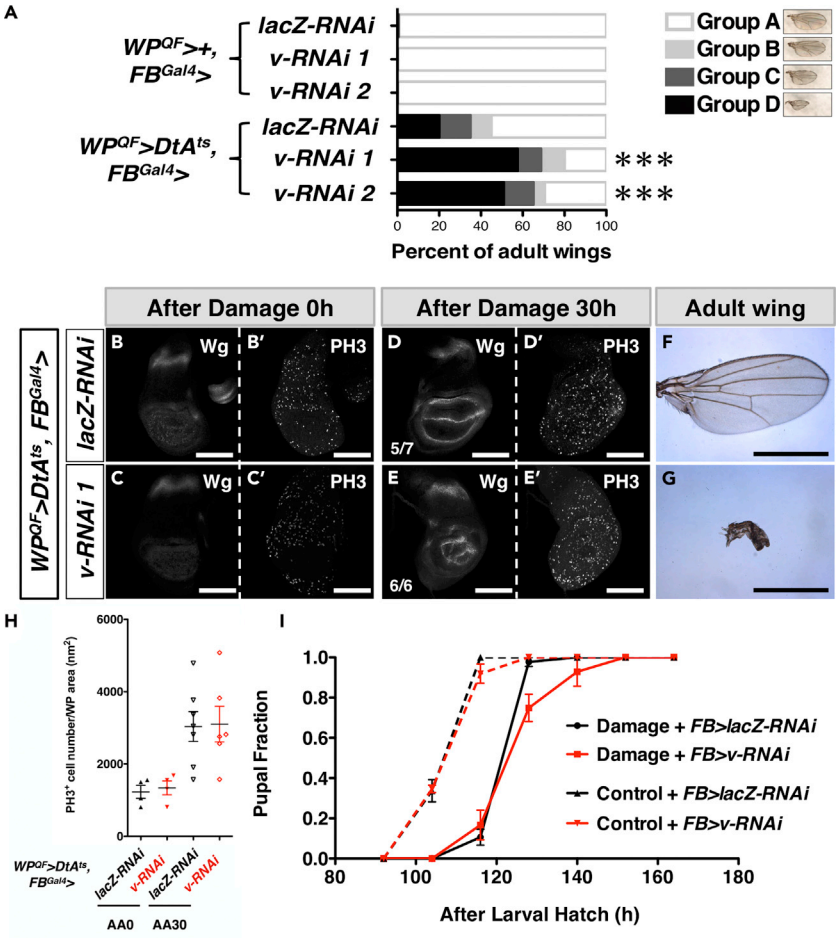

Figure 2. Genetic Manipulation of *Vermilion* in the Fat Body Causes Impairment of Wing Disc Repair

(A) Comparison of adult wing sizes. From top to bottom: WP^{QF}>+, FB^{Gal4}>*lacZ-RNAi* (n = 154); WP^{QF}>+, FB^{Gal4}>*v-RNAi 1* (n = 144); WP^{QF}>+, FB^{Gal4}>*v-RNAi 2* (n = 216); WP^{QF} > DtA^{ts}, FB^{Gal4}>*lacZ-RNAi* (n = 60); WP^{QF} > DtA^{ts}, FB^{Gal4}>*v-RNAi 1* (n = 80); and WP^{QF} > DtA^{ts}, FB^{Gal4}>*v-RNAi 2* (n = 112). Statistical analysis was conducted using the chi-square test to compare the control (WP^{QF}>+, DtA^{ts}, FB^{Gal4}>+) with the treatment larvae; ***, $p < 0.001$.

(B-E') Representative examples of wing discs developed within the indicated time course: WP^{QF}>DtA^{ts}, FB^{Gal4}>*lacZ-RNAi* (B, B', D, and D') and WP^{QF}>DtA^{ts}, FB^{Gal4}>*v-RNAi 1* (C, C', E, and E').

(F and G) Representative example of adult wings of Group A of WP^{QF} > DtA^{ts}, FB^{Gal4}>*lacZ-RNAi*, and Group D of WP^{QF} > DtA^{ts}, FB^{Gal4}>*v-RNAi 1*. Black scale bar, 1 mm.

(H) PH3 positive cell numbers in the wing pouch region was quantified. Samples were same as Figure 2B', C', D' and E'. n = 4, 4, 7, and 6 for each sample. Error bars indicate standard error of the mean.

(I) Timing of pupation for "Control + FB^{Gal4}>*lacZ-RNAi*" larvae (WP^{QF}>+, FB^{Gal4}>*lacZ-RNAi*), "Control + FB^{Gal4}>*v-RNAi*" larvae (WP^{QF}>+, FB^{Gal4}>*v-RNAi 1*), "Damage + FB^{Gal4}>*lacZ-RNAi*" larvae (WP^{QF}>DtA^{ts}, FB^{Gal4}>*lacZ-RNAi*), and "Damage + FB^{Gal4}>*v-RNAi*" larvae (WP^{QF}>DtA^{ts}, FB^{Gal4}>*v-RNAi 1*). n = 60, 73, 38, and 35, respectively. SEM was calculated from four repeated experiments. Developmental timing is represented as both the fraction of total larvae pupated and hours after larval hatch. Temperature treatment was described in Materials and Methods.

remodeling are involved in disc repair (Cosolo et al., 2019; Iida et al., 2019; Yoo et al., 2016). Notably, *vermilion* knockdown in the FB affected tissue structure and dying cells clearance (Figures S4A and S4B). At AA30, regenerative discs indicated the basal extrusion of dying cells; dying cells were accumulated throughout the discs, and the tissue structure was winding, establishing excess folds in non-regenerative discs (Figures S4A and S4B). We also quantified the Dcp1 signals in a projected XZ cross section of wing discs and found that dying cells or debris exist on relatively apical sides of discs compared with *lacZ* knockdown larvae (Figure S4A', S4B', and S4C). Additionally, the intensity of Dcp1 in the WP region did not show a significant difference between regenerative and non-regenerative discs (Figure S4D), implying that the amount of dying cells was not significantly increased by Trp-Kyn metabolism impairment.

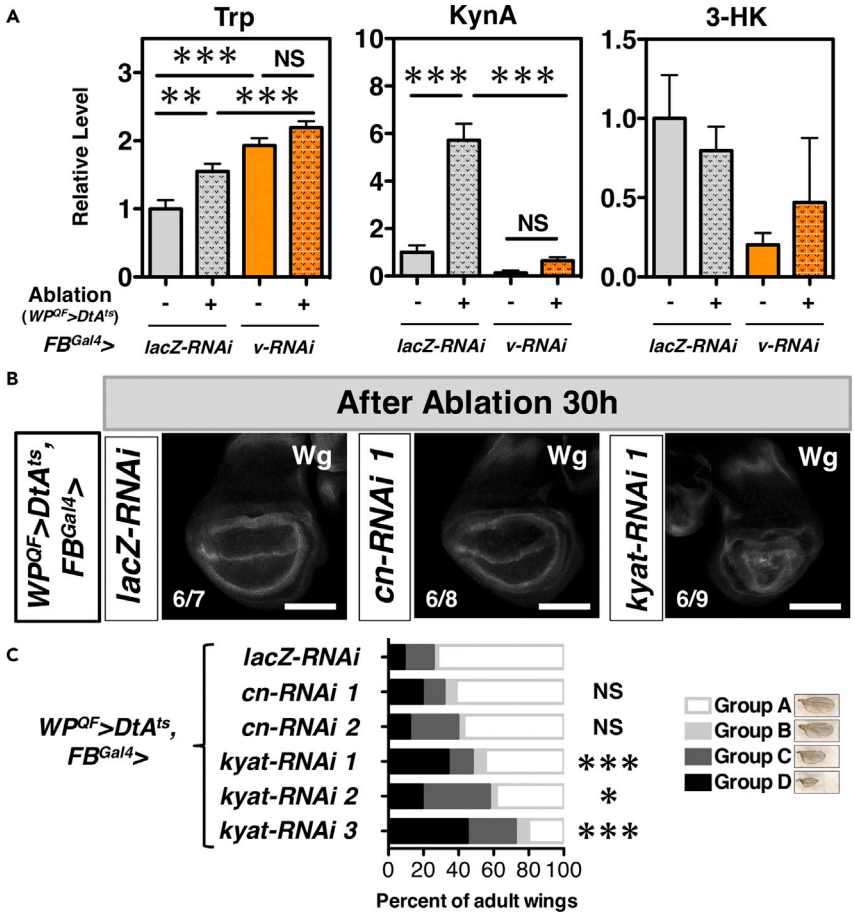

Figure 3. Humoral KynA from the FB Is Required for Disc Repair

(A) The levels of Trp, KynA, and 3-HK in the disc-cell-ablated and non-ablated larval hemolymph with FB-specific RNAi of *lacZ* or *v* at AA6. The metabolites were measured with UPLC-MS/MS. SEM was calculated from four to five independent samples. One-way ANOVA Tukey's multiple comparison test was applied: NS, not significant; **, $p < 0.01$; ***, $p < 0.001$.

(B) Representative examples of wing discs developed within the indicated time course. The discs were stained with anti-Wg. White scale bar, 100 μm.

(C) Comparison of adult wing sizes when Trp-Kyn enzymes are manipulated with the *FB-Gal4* driver. n = 78, 88, 58, 94, 46, and 40 for each sample from top to bottom. Statistical analysis was conducted using the chi-square test to compare the control (WP^{QF} > DtA^{ts}, FB^{Gal4}>*lacZ-RNAi*) with the treatment larvae; NS, not significant; *, $p < 0.05$; ***, $p < 0.001$.

Humoral KynA Derived from the FB Is Required for Disc Repair

To narrow down the metabolites responsible for disc repair, we measured Trp-Kyn metabolites in the hemolymph at the early stage of disc repair (AA6) using LC-MS/MS. As for Trp, the amount of Trp at AA6 in cell-ablated larval hemolymph was the same given by the metabolome analysis (Figure 1A), and *v-RNAi* caused a higher amount of Trp in the hemolymph (Figure 3A). Importantly, the KynA level, and not that of 3-HK, was higher in the cell-ablated condition at AA6 and significantly decreased in *v-RNAi* larval hemolymph (Figure 3A). Furthermore, FB-specific knockdown of *Kynurenine aminotransferase* (*Kyat*), a gene required for KynA synthesis (Figure 1A), caused a severe wing disc phenotype (Figure 3B), and adults showed a worse wing phenotype compared with the knockdowns of *cinnabar* (*cn*), a kynurenine 3-monooxygenase (KMO) producing 3-HK (Figures 3C and S5B). Therefore, these results indicated that KynA synthesis in the FB was required for disc repair.

To investigate the requirement of humoral KynA for disc repair, an oral KynA feeding experiment was conducted (Figure 4A). KynA administration from AA0 rescued the level of humoral KynA of *vermilion* knockdown larvae (Figure 4B). Furthermore, the severe wing phenotype was also recovered via KynA feeding (Figures 4D and S5E), and KynA treatment also decreased the population of severe Wg phenotype (Class

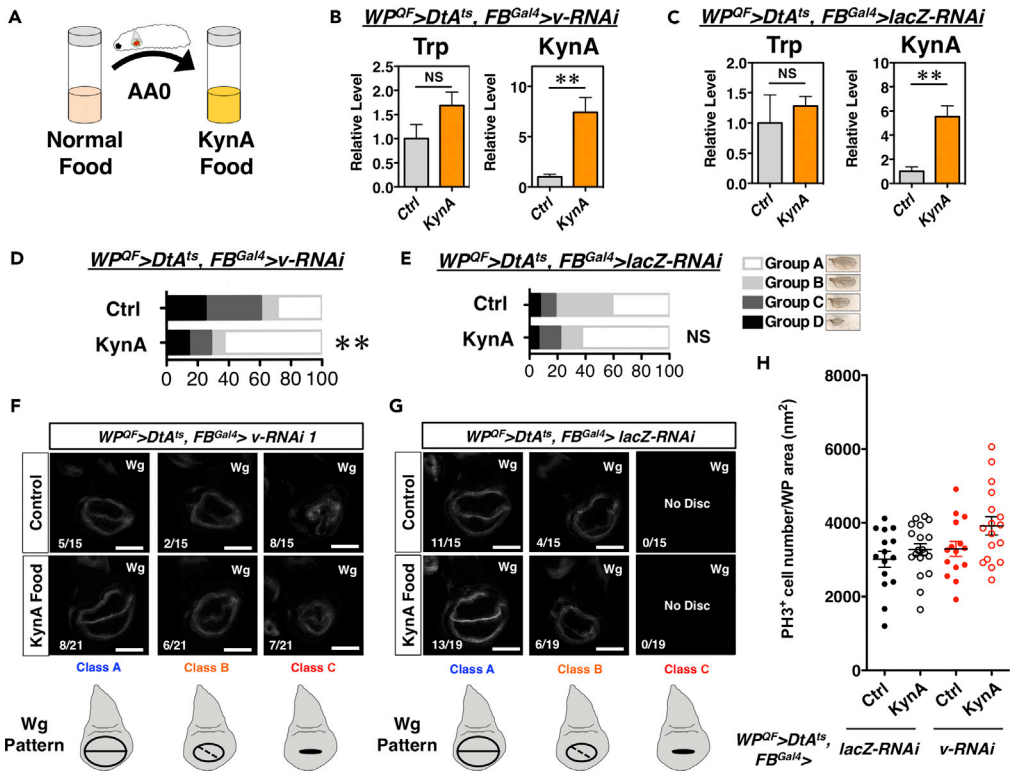

Figure 4. Oral KynA Administration Rescues Disc Repair in Trp-Kyn Metabolism-Impaired Larvae

(A) Schematic view of KynA administration.

(B) The levels of Trp and KynA in ablated and *v* knockdown (*v-RNAi 1*) larval hemolymph at AA6 under the KynA administration condition. Error bars represent the SEM, and p-values were calculated using the two-tailed student's *t*-tests. SEM was calculated from six independent samples; NS, not significant; **p < *0.01*.

(C) The levels of Trp and KynA in ablated and *lacZ* knockdown larval hemolymph at AA6 under the KynA administration condition. Error bars represent the SEM, and p-values were calculated using the two-tailed student's *t*-tests. SEM was calculated from six independent samples; NS, not significant; **p < *0.01*.

(D) Comparison of adult wing sizes in the condition of *v* knockdown in the fat body with or without KynA administration. n = 56 and 70. Chi-squared test to compare control with KynA treated larvae; **p < *0.01*.

(E) Comparison of adult wing sizes in the condition of *lacZ* knockdown in the fat body with or without KynA administration. n = 54 and 32. Chi-squared test to compare control with KynA treated larvae; NS, not significant.

(F and G) Representative example of wing discs at AA30: $WP^{QF}>DtA^{ts}$, FB^{Gal4}>*v-RNAi 1* (F) and $WP^{QF}>DtA^{ts}$, FB^{Gal4}>*lacZ-RNAi* (G).

(H) PH3 positive cell numbers in the wing pouch region were quantified. n = 15, 19, 15, and 17. Error bars indicate standard error of the mean.

C) of the FB-specific *vermilion-RNAi* larval disc (Figure 4F). Because KynA is an end product of the Trp-Kyn pathway, these results suggested the requirement of humoral KynA, rather than in the FB tissue, for disc repair. On the other hand, KynA treatment did not enhance the regenerating phenotype of FB-specific *lacZ-RNAi* larval discs and adult wings (Figures 4C, 4E, 4G and S5F), possibly because humoral KynA level in damaged control larvae was saturated to supporting disc repair. As for PH3 staining, KynA treatment did not increase the number of PH3-positive cells in the WP region of either FB-specific *lacZ-RNAi* or *vermilion-RNAi* larvae (Figure 4H), which was accompanied with the results of no apparent effects of *vermilion-RNAi* in the FB on PH3 (Figures 2B–2E and 2H).

Impairment of SAM Synthesis in the FB Represses the Level of Kyn and KynA at the Early Stage of Disc Repair

In addition to the Trp-Kyn pathway, another major metabolic pathway in the FB is the Met-SAM pathway (Kashio et al., 2017). Our previous study indicated that the expression level of SAM synthase (*sams*) was up-regulated in the FB of disc-cell-ablated larvae at AA6 and that *sams* in the FB was required for disc

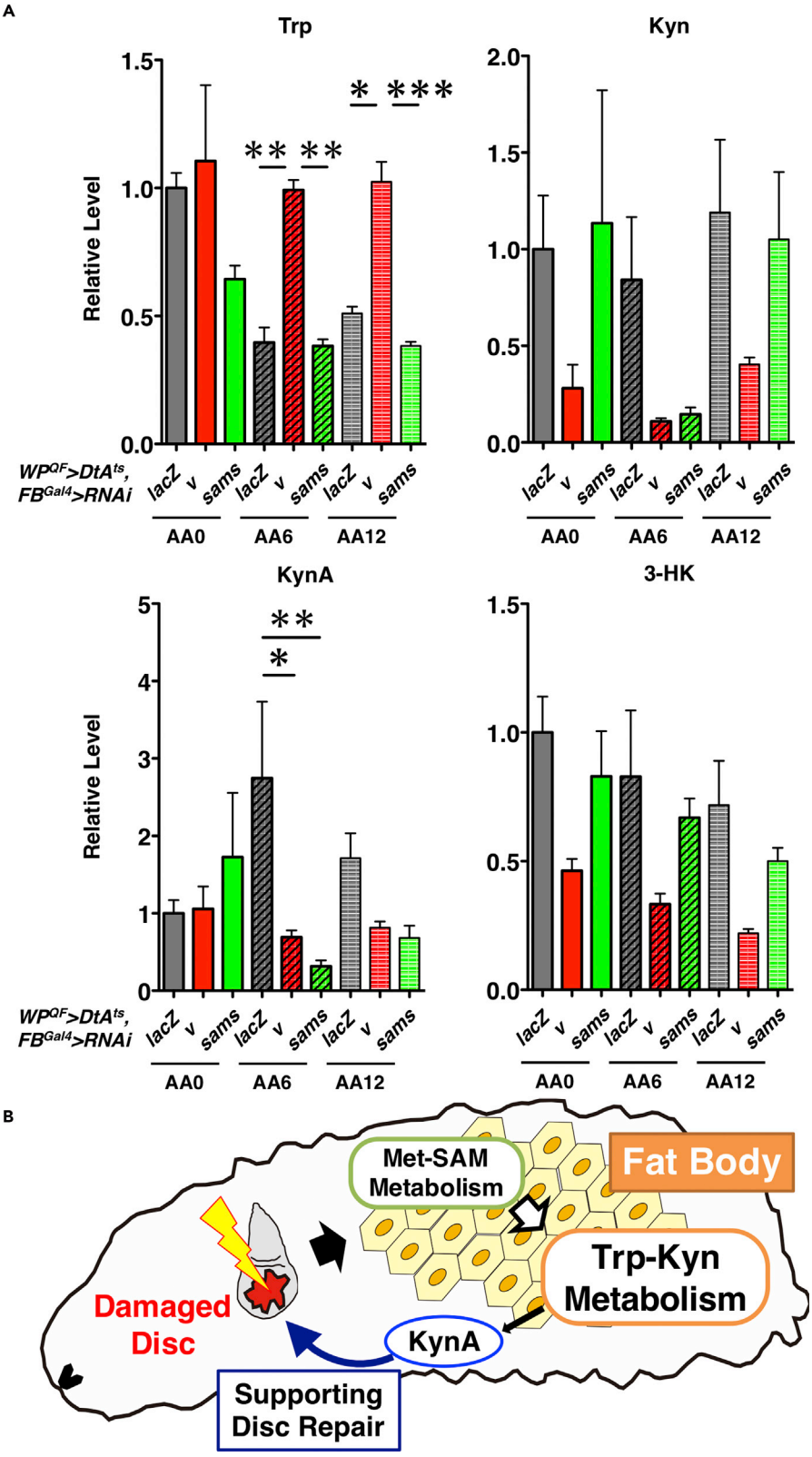
A
Trp
Kyn
KynA
3-HK
Relative Level
WPQF>DtATs,
FBGal4>RNAi
lacZ
v
sams
AA0
AA6
AA12
B
Met-SAM Metabolism
Fat Body
Trp-Kyn Metabolism
KynA
Damaged Disc
Supporting Disc Repair

Figure 5. Met-SAM and Trp-Kyn Pathways in the FB Remotely Regulate Disc Repair via Humoral KynA

(A) The levels of Trp, Kyn, KynA, and 3-HK in disc-ablated larval hemolymph with FB-specific RNAi of *lacZ*, *v* (*v-RNAi 1*), or *sams* at AA0, 6, and 12. The metabolites were measured using UPLC-MS/MS. SEM was calculated from five to six independent samples. One-way ANOVA Tukey's multiple comparison test was applied: *, $p < 0.05$; **, $p < 0.01$; ***, $p < 0.001$.

(B) Scheme of the tissue nonautonomous effects of Met-SAM and Trp-Kyn metabolisms in the fat body on repairing disc via KynA.

regeneration (Kashio et al., 2016). Therefore, we wondered whether there were any interrelationships between these two major metabolic pathways in the FB. We compared the metabolic changes of FB-specific *vermilion* or *sams* knockdown larval hemolymph at AA0, 6, and 12 (Figure 5A). *Vermilion* knockdown resulted in the highest level of Trp compared with the control, but *sams* knockdown did not present the same results as the *vermilion* knockdown. On the other hand, the downregulation of KynA in both the *vermilion* and *sams* knockdowns was observed at AA6 (a similar tendency was also observed at AA12). As for Kyn and 3-HK, *vermilion* knockdown tended to repress the level of Kyn or 3-HK at all time points, whereas the *sams* knockdown showed almost the same levels as the control, besides a decreasing tendency of Kyn at AA6. From these results, we assumed that Sams is required in the FB for the maintenance of KynA in the early stage of disc repair (Figure 5B).

DISCUSSION

In the context of organ communications, peptides or secreted proteins are mainly studied as signaling molecules (Droujinine and Perrimon, 2016), even though small molecules like metabolites have several other advantages, such as the possibility of rapid diffusion or transcellular transport. In this paper, we focused on metabolites as inter-tissue mediators. Trp-derived metabolites function in diverse situations. As for tissue regeneration, a recent planarian study implied the involvement of indole, a Trp catabolite via the microbiome, impaired regeneration (Lee et al., 2018). Ischemia by cardiac arrest is reported to change the plasma KynA level in rats, pigs, and humans (Ristagno et al., 2013), and a study reported that KynA has a protective effect against ischemic tissue damage (Olenchock et al., 2016), which supports our idea that KynA regulates tissue repair non-autonomously. Even though the concrete mechanisms are still under investigation, such functions imply the multifactorial mechanisms of Trp metabolites on tissue repair and regeneration.

The reason why humoral Trp level was higher in AA6 of disc damaged larvae was also unclear. During normal development of larvae, both Met and Trp metabolites gradually decrease from mid-larval stage at a whole-body level (Figure S2F) (Kashio et al., 2016). Considering that developmental progression decreases the regenerative capacity of discs autonomously (Narbonne-Reveau and Maurange, 2019), this implies that a damage-induced developmental delay maintained the level of humoral Trp in regenerating larvae. Besides the effects of developmental delay, it also indicated that plasma free Trp is increased under fatigue conditions in mammals. For example, exercise increased the plasma free Trp in rats, which is associated with an increase of plasma nonesterified fatty acid (NEFA) competing for binding to albumin with Trp (Fernstrom and Fernstrom, 2006). Considering this point, we can also assume that disc injury causes some stresses like fatigue, which increases the amount of Trp in larval hemolymph during disc repair. Additionally, the gut in disc-damaged larva showed a lower level of Trp at AA6 (Figure S2C), which implied that the intake of Trp from gut to hemolymph possibly affected humoral Trp level. Furthermore, considering that Trp is the lowest-frequency amino acid in eukaryote proteins (Id et al., 2019), the lower usage of Trp for protein synthesis at the early stage of disc repair is also one of the possible causes of the humoral level of Trp. Future studies are required for the trigger of Trp-Kyn pathway changes during disc repair.

Several targets of KynA were studied in various biological contexts. As for NMDAR, α7nAChR, or glutamate receptor (GluR), the neural activation of these receptors is repressed by the allosteric binding of KynA (Schwarcz et al., 2012; Wirthgen et al., 2018). Several papers indicated that GPR35 is a target of KynA, even though a paper also showed an undetectable binding capacity of KynA to GPR35 (Inoue et al., 2012). For instance, muscle-derived KynA increased energy expenditure by activating GPR35 (Agudelo et al., 2018). KynA was also reported as a potent AhR endogenous ligand that could induce interleukin-6 (IL-6) production and xenobiotic metabolism (DiNatale et al., 2010). For transportation of KynA into cells, human organic anion transporters hOAT1 (SLC22A6) and hOAT3 (SLC22A8) mediate the transport of KynA using a *Xenopus laevis* oocyte expression system (Uwai et al., 2012). So far, there are no reports about the

obvious way to use KynA in *Drosophila*. Furthermore, it is still unclear if KynA acts in disc repair directly or indirectly; thus, further studies seeking the KynA target are needed.

Our results also suggested interactions between Met-SAM and Trp-Kyn metabolism in the early stage of disc regeneration. Although the nature of the connection between SAM synthesis and tryptophan catabolism during disc repair is still unclear, the enzymatic activity in the Trp-Kyn pathway could be affected by Met or SAM level. Mouse kynurenine aminotransferase III (KAT III) that catalyzes the transamination of Kyn to KynA is effectively inhibited by Met *in vitro* (Han et al., 2009). We previously showed that *sams* knockdown in larval fat body significantly increased Met level (Kashio et al., 2016); thus, *Drosophila* Kyat activity might be suppressed and the KynA production could be reduced in *sams* knockdown condition.

Previous studies indicated the enzymatic regulatory mechanisms by methylation, for example, it has been reported that methylation of the catalytic subunit in protein phosphatase 2 A (PP2A) keeps the phosphatase activity by hampering the binding of TOR signaling pathway regulator (TIPRL), which binds to the demethylated PP2A and disassembles holoenzyme (Wu et al., 2017). Additionally, Lys 260 methylation in MAPK kinase kinase 2 (MAP3K2) blocks the interaction with its negative regulator PP2A, leading to an increase in the activity of MAP/ERK kinase 1 (MEK1) and MEK2 (Mazur et al., 2014). Even though it has not been investigated whether enzymatic activity or gene expression in the Trp-Kyn pathway is regulated by SAM, including the involvement of PP2A and MAP3K2, further biochemical experiments will be needed for the requirement of methylation on the regulation of enzymes in Trp-Kyn pathway.

Correlation of Met-SAM and Trp-Kyn metabolism changes in several biological processes has been reported. As for the regulation of pluripotency in human embryonic stem cells (hESCs), both the Kyn/Trp ratio and SAM level is higher in primed than in naive hESCs (Sperber et al., 2015). It was also indicated that Trp-Kyn metabolites affect histone modification. Although the mechanisms have not been studied, the supplementation of Kyn, 3-HK, and Anthranilate during the neural differentiation from committed human iPSCs induced histone H3 lysine 4 trimethylation (H3K4me3) for maintenance of neural gene expression (Hayakawa et al., 2019). On the other hand, SAM is also required for maintenance of undifferentiated ESC and iPSC and SAM depletion enhanced differentiation (Shiraki et al., 2014), and Kyn catabolism by KMO and KAT II is enhanced during ectodermal differentiation (Yamamoto et al., 2019). Thus, both Trp-Kyn and Met-SAM pathways act in the same direction for regulation of differentiation status. Additionally, glioblastoma shows abnormal Met and Trp-Kyn metabolic changes (Palanichamy et al., 2016). Notably, in the context of aging and the reduction of dietary amino acids, tryptophan and methionine can extend the lifespan in animal models (Fontana and Partridge, 2015). Alzheimer's disease and mild cognitive impairment are associated with an overlapping pattern of perturbations in Trp, tyrosine, Met, and purine pathways (Kaddurah-Daouk et al., 2013). Additionally, both Trp and Met restrictions exert protective effects in ischemia/reperfusion damage (López-Otín et al., 2016). Therefore, further studies on the interconnection of Met and Trp-Kyn metabolisms would be worthy of note in various biological contexts. Since our data suggested the metabolic connection between Met-SAM and Trp-Kyn pathway in the fat body during disc repair, it is the next important research topics to know the regulatory mechanisms of these two pathways for repairing discs.

Limitations of the Study

Compared with the Met-SAM pathway, the Trp-Kyn metabolic pathway is rather simple, and its catabolic pathway proceeds linearly to produce KynA as an end product. We conducted fat body-specific gene manipulation and tissue-specific measurements of metabolites for the Trp-Kyn pathway in this study. Although we found the production of KynA in the FB is required for systemic control of disc repair and regeneration, we could not exactly reveal the dynamics of KynA and whether KynA directly acts on wing imaginal disc or on other tissues. In mammals, KynA can exert its function through binding to NMDAR, a7nAChR, GluR, GPR35, or AhR. Therefore, it is necessary to identify KynA-binding receptors required for disc repair. It is also intriguing to know whether KynA functions in tissue regeneration in other organisms.

Resource Availability

Lead Contact

Further information and requests for resources and reagents should be directed to and will be fulfilled by the Lead Contact, Masayuki Miura (miura@mol.f.u-tokyo.ac.jp).

Materials Availability

Materials and protocols used in this study are available from the authors upon request.

METHODS

All methods can be found in the accompanying Transparent Methods supplemental file.

SUPPLEMENTAL INFORMATION

Supplemental Information can be found online at https://doi.org/10.1016/j.isci.2020.101738.

ACKNOWLEDGMENTS

We thank the Bloomington *Drosophila* Stock Center and Vienna *Drosophila* Resource Center for fly stocks. We thank Dr. Ronald P. Kühnlein for the FB-Gal4 fly. This work was supported by research grants from the Japan Society for the Promotion of Science (grant numbers JP16H06385 to M.M., and 15J12331, 18H06064, and 19K16136 to S.K.). It was also supported by the Japan Agency for Medical Research and Development through AMED-CREST (grant number JP17gm0610004), and AMED-Aging (grant number JP20gm5010001) to M.M., as well as the Graduate Program for Leaders in Life Innovation Leading Graduate School from the Ministry of Education, Culture, Sports, Science and Technology (MEXT), and the Sasakawa Scientific Research Grant from the Japan Science Society to S.K. We thank all members of the Miura laboratory, especially F. Obata and N. Shinoda, for their helpful discussions and comments.

AUTHOR CONTRIBUTIONS

S.K. and M.M. designed the experiments and wrote the paper. S.K. conducted the experiments and analyzed the data.

DECLARATION OF INTERESTS

The authors declare no competing or financial interests.

Received: May 14, 2020
Revised: September 7, 2020
Accepted: October 23, 2020
Published: November 6, 2020

REFERENCES

Agudelo, L.Z., Ferreira, D.M.S., Cervenka, I., Bryzgalova, G., Dadvar, S., Jannig, P.R., Pettersson-Klein, A.T., Lakshmikanth, T., Sustarsic, E.G., Porsmyr-Palmertz, M., et al. (2018). Kynurenic acid and Gpr35 regulate adipose tissue energy homeostasis and inflammation. Cell Metab. *27*, 378–392.

Bellen, H.J., D'Evelyn, D., Harvey, M., and Elledge, S.J. (1992). Isolation of temperature-sensitive diphtheria toxins in yeast and their effects on Drosophila cells. Development *114*, 787–796.

Breda, C., Sathyasaikumar, K.V., Idrissi, S.S., Notarangelo, F.M., Estranero, J.G., Moore, G.G.L., Green, E.W., Kyriacou, C.P., Schwarcz, R., and Giorgini, F. (2016). Tryptophan-2,3-dioxygenase (TDO) inhibition ameliorates neurodegeneration by modulation of kynurenine pathway metabolites. Proc. Natl. Acad. Sci. U S A *113*, 5435–5440.

Cervenka, I., Agudelo, L.Z., and Ruas, J.L. (2017). Kynurenines: tryptophan's metabolites in exercise, inflammation, and mental health. Science *357*, eaaf9794.

Colombani, J., Andersen, D.S., and Leopold, P. (2012). Secreted peptide Dilp8 coordinates Drosophila tissue growth with developmental timing. Science *336*, 582–585.

Cosolo, A., Jaiswal, J., Csordás, G., Grass, I., Uhlirova, M., and Classen, A.K. (2019). JNK-dependent cell cycle stalling in G2 promotes survival and senescence-like phenotypes in tissue stress. Elife *8*, e41036.

DiNatale, B.C., Murray, I.A., Schroeder, J.C., Flaveny, C.A., Lahoti, T.S., Laurenzana, E.M., Omiecinski, C.J., and Perdew, G.H. (2010). Kynurenic acid is a potent endogenous aryl hydrocarbon receptor ligand that synergistically induces interleukin-6 in the presence of inflammatory signaling. Toxicol. Sci. *115*, 89–97.

Droujinine, I.A., and Perrimon, N. (2016). Interorgan communication pathways in physiology: focus on Drosophila. Annu. Rev. Genet. *50*, 539–570.

Fernstrom, J.D., and Fernstrom, M.H. (2006). Exercise, serum free tryptophan, and central fatigue. J. Nutr. *136*, 553S–559S.

Fontana, L., and Partridge, L. (2015). Promoting health and longevity through diet: from model organisms to humans. Cell *161*, 106–118.

Fox, D.T., Cohen, E., and Smith-Bolton, R. (2020). Model systems for regeneration: Drosophila. Development *147*, 0–3.

Garelli, A., Gontijo, A.M., Miguela, V., Caparros, E., and Dominguez, M. (2012). Imaginal discs secrete insulin-like peptide 8 to mediate plasticity of growth and maturation. Science *336*, 579–582.

Halme, A., Cheng, M., and Hariharan, I.K. (2010). Retinoids regulate a developmental checkpoint for tissue regeneration in Drosophila. Curr. Biol. *20*, 458–463.

Han, Q., Robinson, H., Cai, T., Tagle, D.A., and Li, J. (2009). Biochemical and structural properties of mouse kynurenine aminotransferase III. Mol. Cell Biol. *29*, 784–793.

Hayakawa, K., Nishitani, K., and Tanaka, S. (2019). Kynurenine, 3-OH-kynurenine, and anthranilate are nutrient metabolites that alter H3K4 trimethylation and H2AS40 O-GlcNAcylation at hypothalamus-related loci. Sci. Rep. *9*, 1–12.

Id, W.B., Salvatore, M., Id, C.B., and Id, A.E. (2019). Why do eukaryotic proteins contain more intrinsically disordered regions ? Plos Comput. Biol. *15*, e1007186.

Iida, C., Ohsawa, S., Taniguchi, K., Yamamoto, M., Morata, G., and Igaki, T. (2019). JNK-mediated Slit-Robo signaling facilitates epithelial wound repair by extruding dying cells. Sci. Rep. *9*, 19549.

Inoue, A., Ishiguro, J., Kitamura, H., Arima, N., Okutani, M., Shuto, A., Higashiyama, S., Ohwada, T., Arai, H., Makide, K., et al. (2012). TGFα shedding assay: an accurate and versatile method for detecting GPCR activation. Nat. Methods *9*, 1021–1029.

Johnson, K., Bateman, J., DiTommaso, T., Wong, A.Y., and Whited, J.L. (2018). Systemic cell cycle activation is induced following complex tissue injury in axolotl. Dev. Biol. *433*, 461–472.

Kaddurah-Daouk, R., Zhu, H., Sharma, S., Bogdanov, M., Rozen, S.G., Matson, W., Oki, N.O., Motsinger-Reif, A.A., Churchill, E., Lei, Z., et al. (2013). Alterations in metabolic pathways and networks in Alzheimer's disease. Transl. Psychiatry *3*, e244.

Kashio, S., Obata, F., Zhang, L., Katsuyama, T., Chihara, T., and Miura, M. (2016). Tissue nonautonomous effects of fat body methionine metabolism on imaginal disc repair in *Drosophila*. Proc. Natl. Acad. Sci. U S A *113*, 1835–1840.

Kashio, S., Obata, F., and Miura, M. (2017). How tissue damage MET metabolism: regulation of the systemic damage response. Fly (Austin) *11*, 27–36.

Lee, W.J., and Miura, M. (2014). Mechanisms of systemic wound response in Drosophila. Curr. Top. Dev. Biol. *108*, 153–183.

Lee, F.J., Williams, K.B., Levin, M., and Wolfe, B.E. (2018). The bacterial metabolite indole inhibits regeneration of the planarian flatworm dugesia japonica. iScience *10*, 135–148.

Lee, J.W., Cho, E., Aghaian, E., Aghaian, E., Der, J., and Wisnieski, B.J. (2005). Characterization of a cloned temperature-sensitive construct of the diphtheria toxin A domain. Biochemistry *44*, 2555–2565.

Leopold, P., and Perrimon, N. (2007). Drosophila and the genetics of the internal milieu. Nature *450*, 186–188.

López-Otín, C., Galluzzi, L., Freije, J.M.P., Madeo, F., and Kroemer, G. (2016). Metabolic control of longevity. Cell *166*, 802–821.

Mazur, P.K., Reynoird, N., Khatri, P., Jansen, P.W.T.C., Wilkinson, A.W., Liu, S., Barbash, O., Van Aller, G.S., Huddleston, M., Dhanak, D., et al. (2014). SMYD3 links lysine methylation of MAP3K2 to Ras-driven cancer. Nature *510*, 283–287.

Narbonne-Reveau, K., and Maurange, C. (2019). Developmental regulation of regenerative potential in Drosophila by ecdysone through a bistable loop of ZBTB transcription factors. Plos Biol. *17*, e3000149.

Olenchock, B.A., Moslehi, J., Baik, A.H., Davidson, S.M., Williams, J., Gibson, W.J., Pierce, K.A., Miller, C.M., Hanse, E.A., Kelekar, A., et al. (2016). EGLN1 inhibition and rerouting of α-ketoglutarate suffice for remote ischemic protection. Cell *164*, 884–895.

Palanichamy, K., Thirumoorthy, K., Kanji, S., Gordon, N., Singh, R., Jacob, J.R., Sebastian, N., Litzenberg, K.T., Patel, D., Bassett, E., et al. (2016). Methionine and kynurenine activate oncogenic kinases in glioblastoma, and methionine deprivation compromises proliferation. Clin. Cancer Res. *22*, 3513–3523.

Riabinina, O., Luginbuhl, D., Marr, E., Liu, S., Wu, M.N., Luo, L., and Potter, C.J. (2015). Improved and expanded Q-system reagents for genetic manipulations. Nat. Methods *12*, 219–222.

Ristagno, G., Fries, M., Brunelli, L., Fumagalli, F., Bagnati, R., Russo, I., Staszewsky, L., Masson, S., Li Volti, G., Zappalà, A., et al. (2013). Early kynurenine pathway activation following cardiac arrest in rats, pigs, and humans. Resuscitation *84*, 1604–1610.

Rodgers, J.T., Schroeder, M.D., Ma, C., and Rando, T.A. (2017). HGFA is an injury-regulated systemic factor that induces the transition of stem cells into GAlert. Cell Rep. *19*, 479–486.

Schwarcz, R., Bruno, J.P., Muchowski, P.J., and Wu, H.Q. (2012). Kynurenines in the mammalian brain: when physiology meets pathology. Nat. Rev. Neurosci. *13*, 465–477.

Shiraki, N., Shiraki, Y., Tsuyama, T., Obata, F., Miura, M., Nagae, G., Aburatani, H., Kume, K., Endo, F., and Kume, S. (2014). Methionine metabolism regulates maintenance and differentiation of human pluripotent stem cells. Cell Metab. *19*, 780–794.

Sperber, H., Mathieu, J., Wang, Y., Ferreccio, A., Hesson, J., Xu, Z., Fischer, K.A., Devi, A., Detraux, D., Gu, H., et al. (2015). The metabolome regulates the epigenetic landscape during naive-to-primed human embryonic stem cell transition. Nat. Cell Biol. *17*, 1523–1535.

Stone, T.W., Stoy, N., and Darlington, L.G. (2013). An expanding range of targets for kynurenine metabolites of tryptophan. Trends Pharmacol. Sci. *34*, 136–143.

Uwai, Y., Honjo, H., and Iwamoto, K. (2012). Interaction and transport of kynurenic acid via human organic anion transporters hOAT1 and hOAT3. Pharmacol. Res. *65*, 254–260.

Wirthgen, E., Hoeflich, A., Rebl, A., and Günther, J. (2018). Kynurenic Acid: the Janus-faced role of an immunomodulatory tryptophan metabolite and its link to pathological conditions. Front. Immunol. *8*, 1957.

Worley, M.I., Setiawan, L., and Hariharan, I.K. (2012). Regeneration and transdetermination in Drosophila imaginal discs. Annu. Rev. Genet. *46*, 289–310.

Wu, C.G., Zheng, A., Jiang, L., Rowse, M., Stanevich, V., Chen, H., Li, Y., Satyshur, K.A., Johnson, B., Gu, T.J., et al. (2017). Methylation-regulated decommissioning of multimeric PP2A complexes. Nat. Commun. *8*, 2272.

Yamamoto, T., Hatabayashi, K., Arita, M., Yajima, N., Takenaka, C., Suzuki, T., Takahashi, M., Oshima, Y., Hara, K., Kagawa, K., et al. (2019). Kynurenine signaling through the aryl hydrocarbon receptor maintains the undifferentiated state of human embryonic stem cells. Sci. Signal *12*, eaaw3306.

Yoo, S.K., Starnes, T.W., Deng, Q., and Huttenlocher, A. (2011). Lyn is a redox sensor that mediates leukocyte wound attraction in vivo. Nature *480*, 109–112.

Yoo, S.K., Pascoe, H.G., Pereira, T., Kondo, S., Jacinto, A., Zhang, X., and Hariharan, I.K. (2016). Plexins function in epithelial repair in both Drosophila and zebrafish. Nat. Commun. *7*, 12282.

Zwilling, D., Huang, S.Y., Sathyasaikumar, K.V., Notarangelo, F.M., Guidetti, P., Wu, H.Q., Lee, J., Truong, J., Andrews-Zwilling, Y., Hsieh, E.W., et al. (2011). Kynurenine 3-monooxygenase inhibition in blood ameliorates neurodegeneration. Cell *145*, 863–874.

iScience, Volume *23*

Supplemental Information

Kynurenine Metabolism in the Fat Body Non-autonomously Regulates Imaginal Disc Repair in *Drosophila*

Soshiro Kashio and Masayuki Miura

SUPPLEMENTAL FIGURES

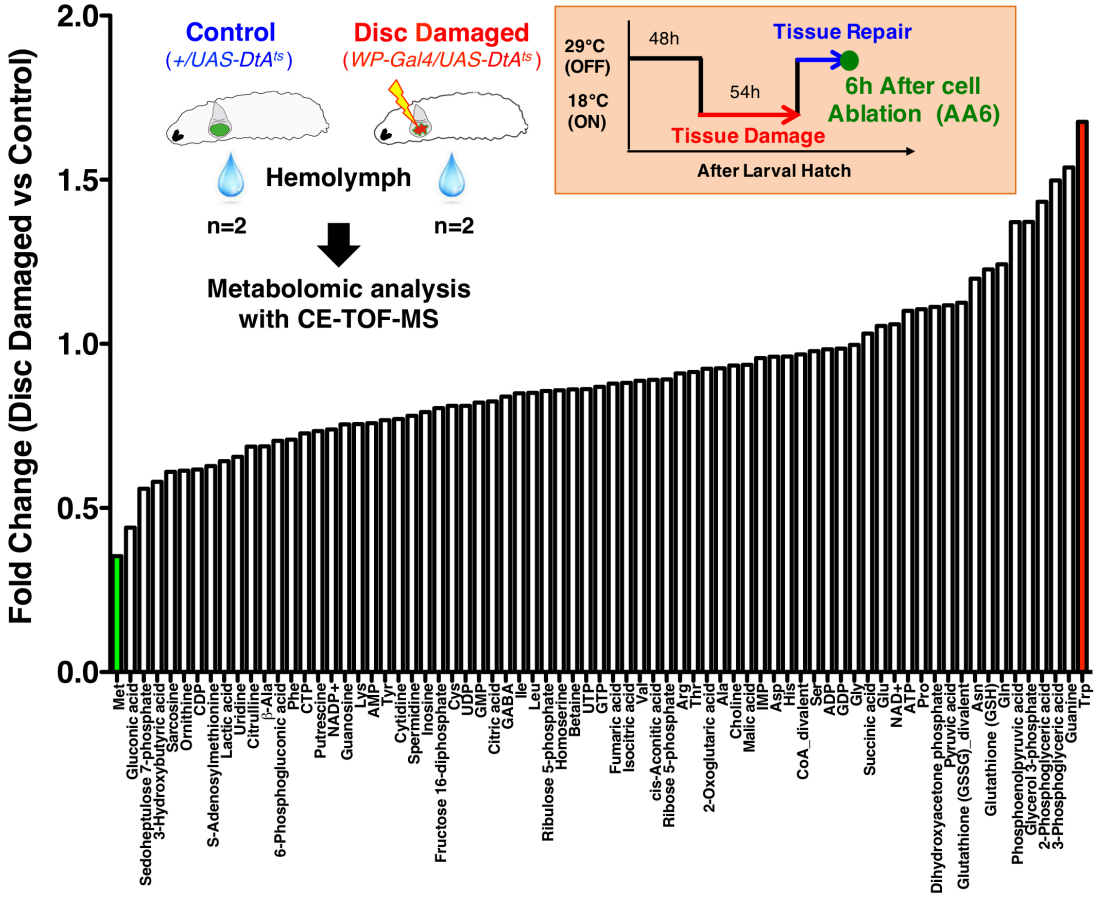

Figure S1. Related to Figure 1. Metabolome analysis of the hemolymph at the early stage of disc repair.

Strategy for metabolome analysis in larval hemolymph from the Control (+/*UAS-DtA*^{ts}) or Disc Damaged (*WP-Gal4/UAS-DtA*^{ts}) samples. Larval hemolymph was collected at the early stage of disc repair (6 h after cell ablation), and metabolome analysis was performed using CE-TOF-MS. Comparison of quantified metabolites between the Control and Ablation samples. Fold change was measured using the mean of duplicates.

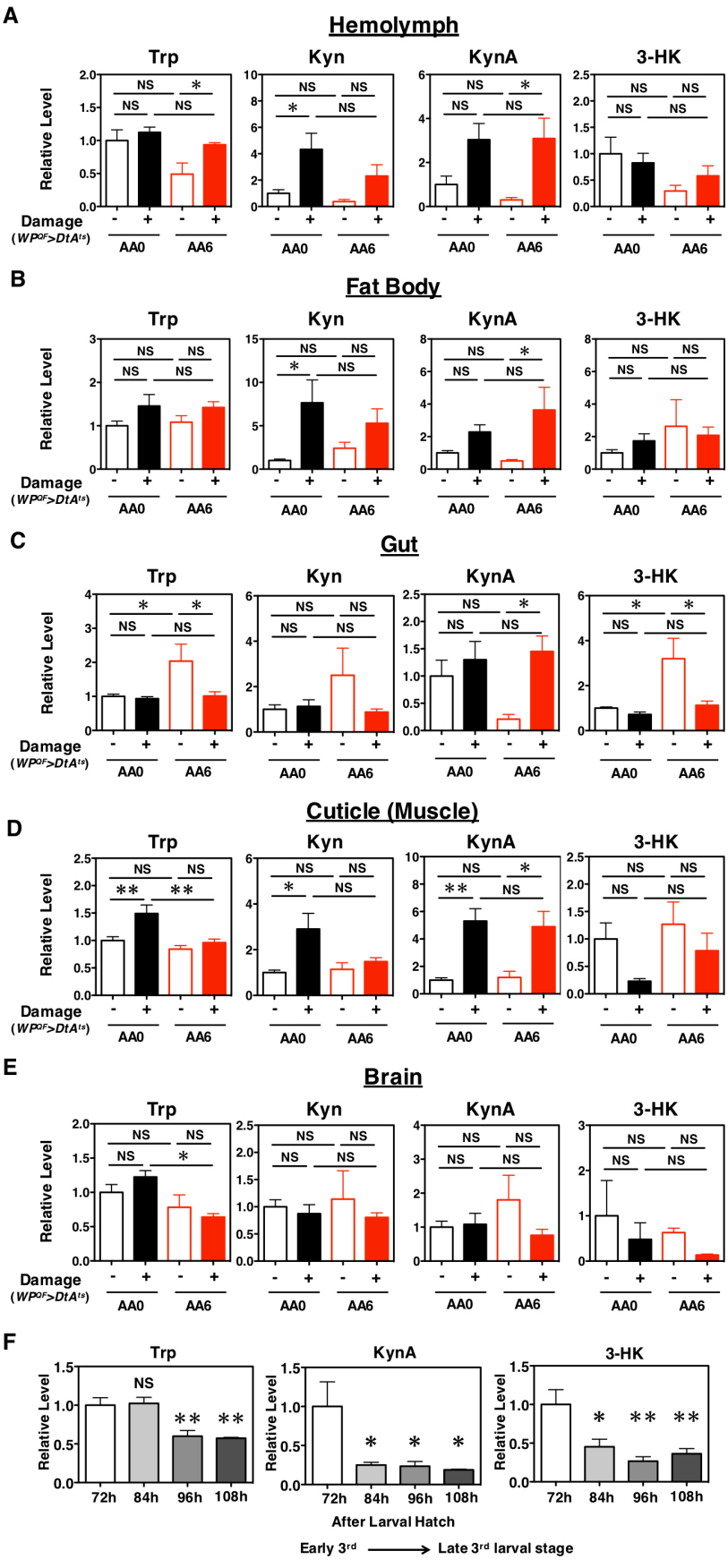
A
Hemolymph
Trp
Kyn
KynA
3-HK
Relative Level
Damage
(WPQF>DtAts)
AA0
AA6
B
Fat Body
C
Gut
D
Cuticle (Muscle)
E
Brain
F
72h
84h
96h
108h
After Larval Hatch
Early 3rd
Late 3rd larval stage

Figure S2. Related to Figure 1. The changes of Trp-Kyn metabolites during the early stage of disc repair and 3rd larval development.

(A-E) The levels of Trp, Kyn, KynA, and 3-HK in the disc-cell ablated (*WP^{QF}>DtA^{ts}, FB^{Gal4}>lacZ-RNAi*) and non-ablated (*WP^{QF}>+, FB^{Gal4}>lacZ-RNAi*) larval hemolymph (A), FB (B), gut (C), cuticle (D), or brain (E) at AA0 and AA6. (F) The levels of Trp, KynA, and 3-HK in whole body wild type larvae (*w^{1118}*) during the 3rd stage of larval development. The metabolites were measured using UPLC-MS/MS. SEM was calculated from 4 independent samples. One-way ANOVA Tukey's multiple comparison test was applied. NS, not significant; *, $p<0.05$; **, $p<0.01$.

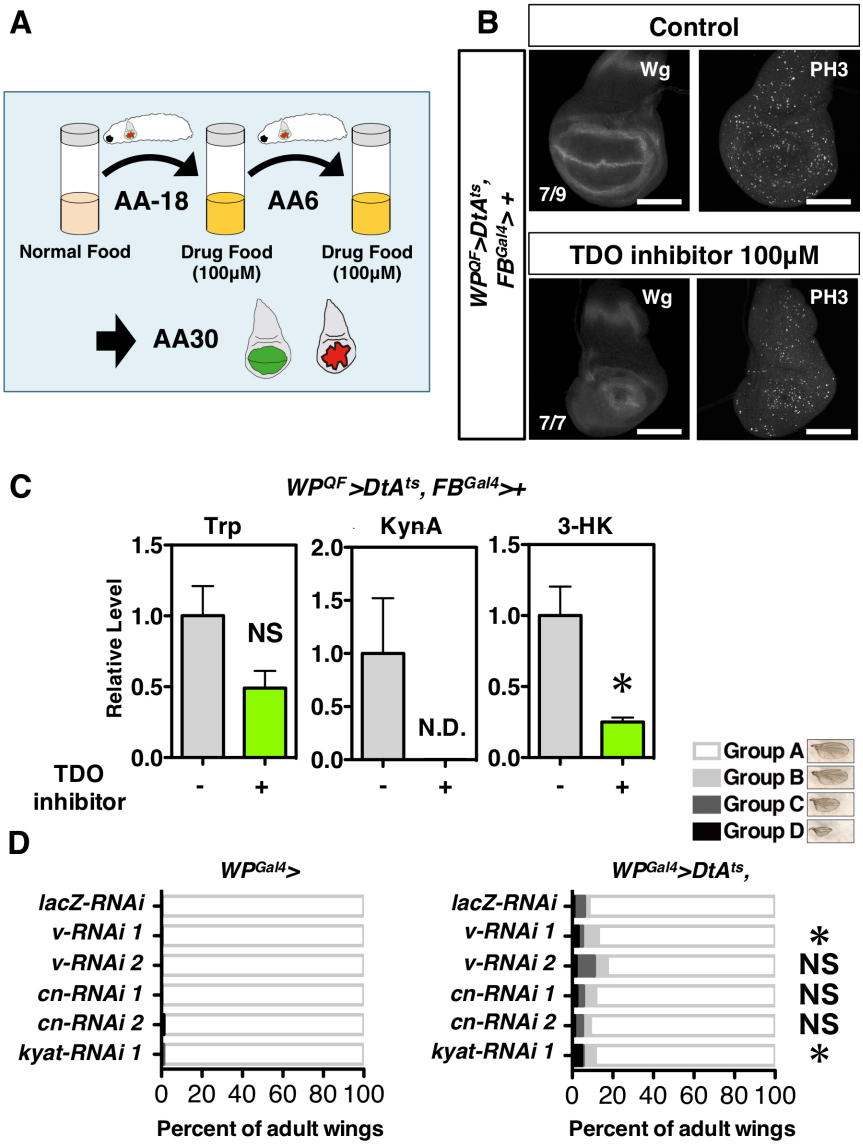

Figure S3. Related to Figure 2. Pharmacological impairment of Vermilion hampers disc repair.
(A) Schematic view of TDO inhibitor administration. (B) Wing discs developed within the indicated time course and food condition. The discs were stained at AA30 with anti-Wg and anti-PH3. White scale bar, 100 μm. (C) The levels of Trp, KynA, and 3-HK in the disc-cell ablated larval hemolymph at AA6 under the TDO inhibitor administrated condition. Error bars represent the SEM, and p-values were calculated using the two-tailed student's; NS, not significant; *, $p<0.05$; N.D., not detected. (D) Comparison of the adult wing sizes in the disc-cell ablated and non-ablated larva. Trp-Kyn pathway genes were manipulated in wing pouch Gal4 driver. n = 220, 252, 246, 160, 164, 190, 134, 140, 110, 182, 180, and 132 for each data from the top left to the bottom right. Statistical analysis was performed using the Chi-squared test; NS, not significant; *, $p<0.05$. Temperature treatment was the same as described in Fig. 1.

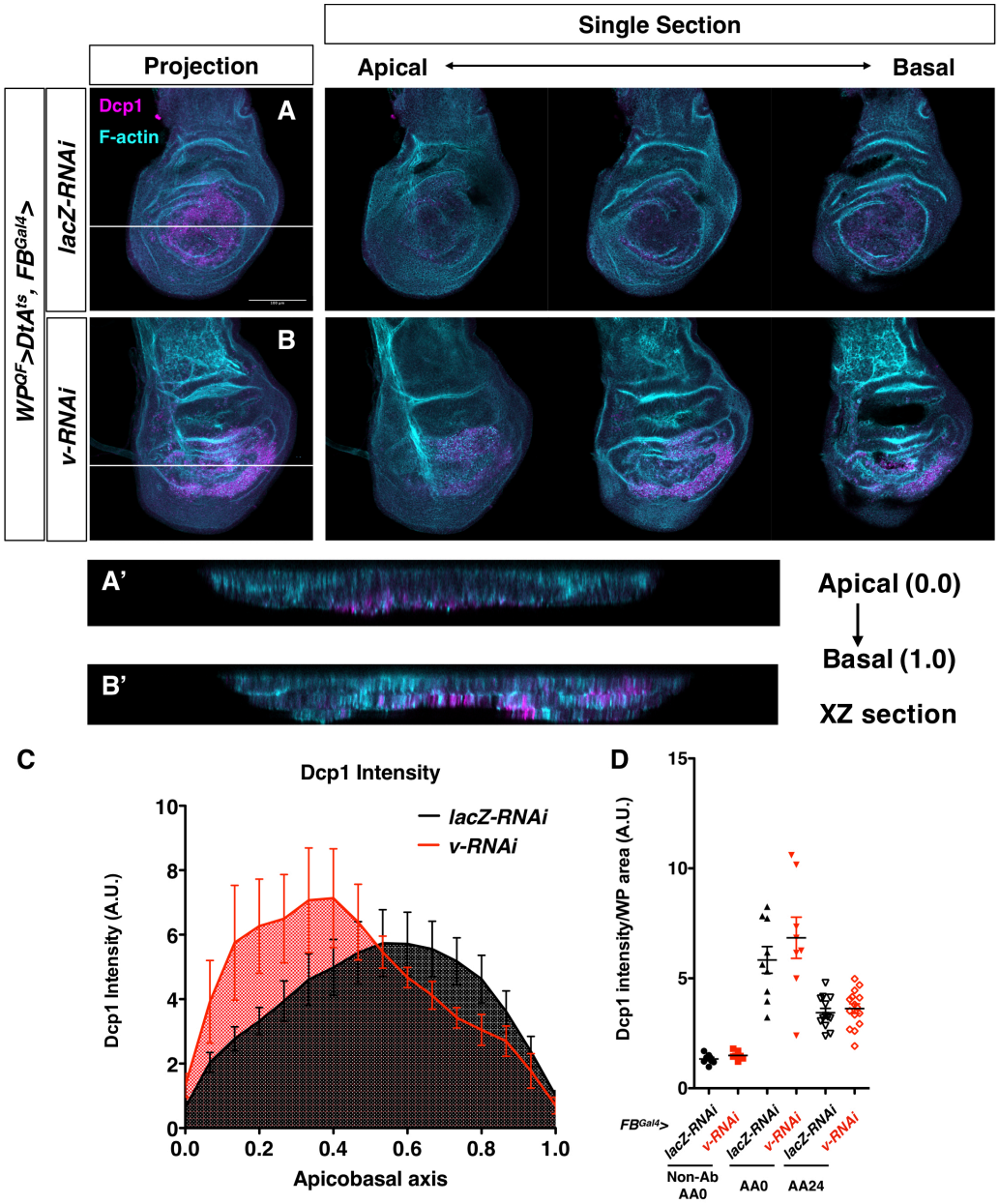

Figure S4. Related to Figure 2. FB-specific knockdown of *vermilion* affects dying cell clearance. (A, B) Section images of regenerative (*WP^{QF}>DtA^{ts}, FB^{Gal4}>lacZ-RNAi*) (A) or non-regenerative (*WP^{QF}>DtA^{ts}, FB^{Gal4}>v-RNAi 1*) (B) discs at AA30. The discs were stained with anti-Dcp1 and phalloidin. White lines indicate the positions of XZ cross-section shown in the bottom panel (A', B'). The discs were stained with anti-Dcp1 and phalloidin. White scale bar, 50 μm. (C) The quantification of Dcp1 signals in projected XZ cross-section of wing discs at AA30. Apicobasal axis (0-1) is indicated from apical to basal. SEM was calculated from four independent samples. (D) Intensity of the Dcp1 signal in wing pouch region was quantified. n = 8, 7, 9, 8, 13, and 15. Error bars indicate standard error of the mean.

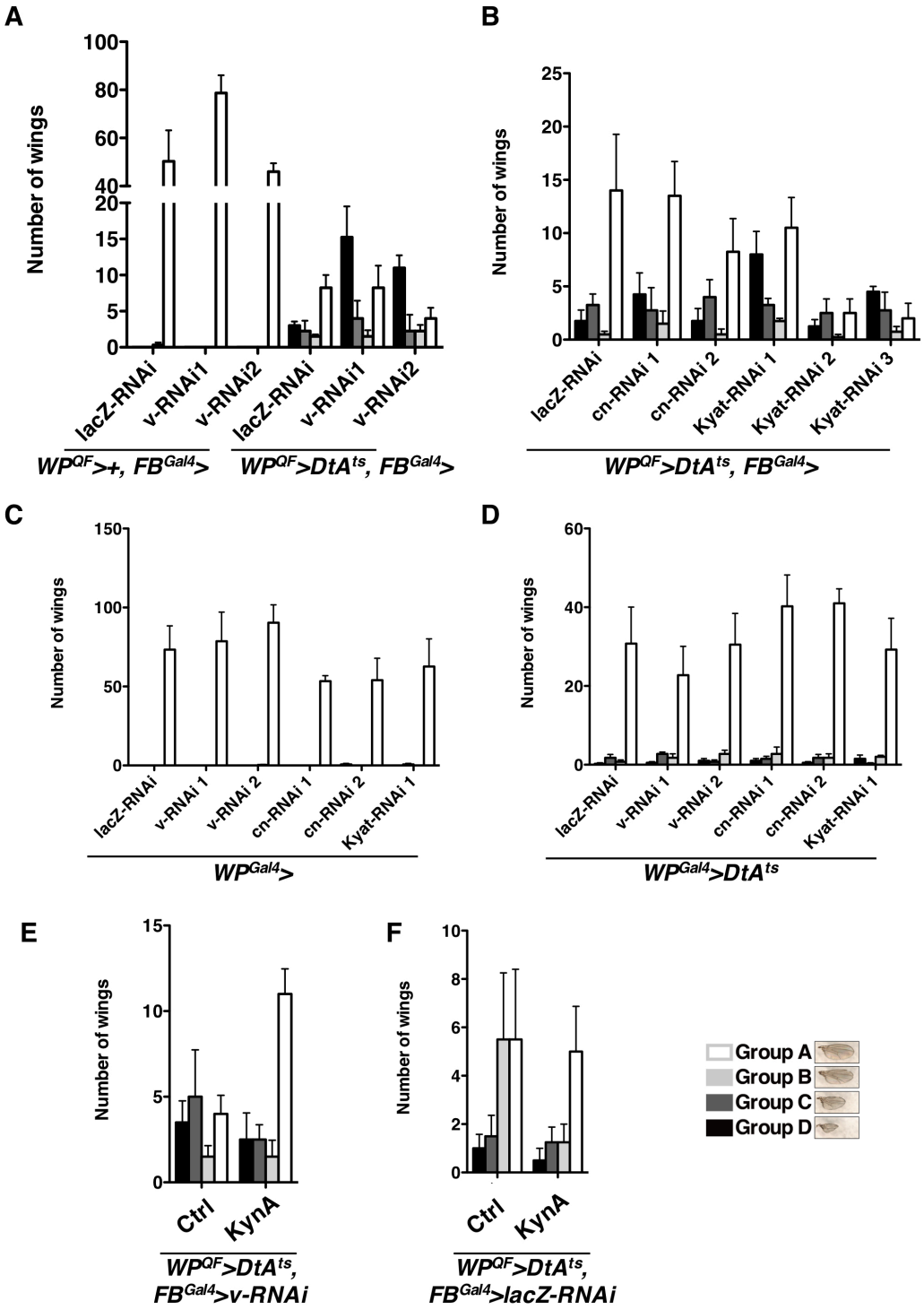

Figure S5. Related to Figures 2, 3, and 4. Reorganized data of adult wing sizes.

Data for comparison of adult wing sizes were reorganized to show the variability across repeats of the experiment. Samples were same as Figure 2A (S5A), 3C (S5B), 4D (S5E), 4E (S5F), and S3D (S5C and S5D). Number of repeated experiments were 4-6. Error bars indicate standard error of the mean.

TRANSPARENT METHODS

KEY RESOURCES TABLE
LEAD CONTACT AND MATERIALS AVAILABILITY
EXPERIMENTAL MODEL AND SUBJECT DETAIL
- Fly Stocks and Transgenes
- Genotype Details

METHOD DETAILS
- Temperature Shift Protocol for Temporal Cell Ablation
- Wing Size Assessment
- Immunohistochemistry
- Metabolome Analysis Using CE-TOF-MS
- Metabolite Extraction from Larval Samples
- UPLC-MS/MS
- Quantitative RT-PCR
- Feeding Experiments

QUANTIFICATION AND STATISTICAL ANALYSIS

KEY RESOURCES TABLE

REAGENT or RESOURCE	SOURCE	IDENTIFIER
Antibodies, Chemicals, and Probes		
rabbit anti-cleaved Dcp1 (Asp216)	Cell Signaling	9578S
mouse anti-Wg	Developmental Studies Hybridoma Bank	4D4
rat anti-GFP (GF090R)	NACALAI TESQUE	04404-26
rabbit anti-PH3 (Ser10)	Millipore	06-570
Hoechst33342	Invitrogen	H3570
Rhodamine Phalloidin	Life technologies	R415
Donkey anti-Rat IgG (H+L) Highly Cross-Adsorbed Secondary Antibody, Alexa Fluor 488	Life Technologies	A-21208
Donkey anti-Mouse IgG (H+L) Highly Cross-Adsorbed Secondary Antibody, Alexa Fluor 647	Life Technologies	A-31571
Cy™3 AffiniPure Donkey Anti-Rat IgG (H+L)	Jackson Immuno Research	712-165-153

Kynurenic acid	SIGMA-ALDRICH	K3375-5G
TDO inhibitor (680C91)	SIGMA-ALDRICH	SML0287-5MG
Fluoromount-G™	SouthernBiotech	00-4958-02
Experimental Models: Organisms/Strains		
D. melanogaster: WP-Gal4	BDSC (Obata et al., 2014)	49828
D. melanogaster: WP-QF2	(Kashio et al., 2016)	N/A
D. melanogaster: UAS-DtA^{ts}	(Kashio et al., 2016)	N/A
D. melanogaster: QUAS-DtA^{ts}	(Kashio et al., 2016)	N/A
D. melanogaster: QUAS-mCD8-GFP	BDSC	30002
D. melanogaster: QUAS-mCD8-GFP	BDSC	30003
D. melanogaster: v^{36f}	BDSC	142
D. melanogaster: FB-Gal4	(Grönke et al., 2003)	N/A
D. melanogaster: UAS-lacZ-RNAi	(Kennerdell and Carthew, 2000)	N/A
D. melanogaster: UAS-v-RNAi	VDRC	3349
D. melanogaster: UAS-v-RNAi	VDRC	107798
D. melanogaster: UAS-cn-RNAi	VDRC	105854
D. melanogaster: UAS-cn-RNAi	VDRC	11322
D. melanogaster: UAS-kyat-RNAi	VDRC	108093
D. melanogaster: UAS-kyat-RNAi	VDRC	22321
D. melanogaster: UAS-kyat-RNAi	VDRC	22322
D. melanogaster: UAS-sams-RNAi	VDRC	103143
Oligonucleotides		
Primers for plasmid construction, see method details	This paper	Method details
Software and Algorithms		
Leica Application Suite X	Leica Microsystems	N/A
ImageJ	National Institutes of Health	N/A
Prism	GraphPad	N/A

LEAD CONTACT AND MATERIALS AVAILABILITY

Further information and requests for resources and reagents should be directed to and will be fulfilled by the Lead Contact, Masayuki Miura (miura@mol.f.u-tokyo.ac.jp).

EXPERIMENTAL MODEL AND SUBJECT DETAIL

Fly Stocks and Transgenes

WP-Gal4, *WP-QF2*, *FB-Gal4*, *UAS-DtA^{ts}*, *QUAS-DtA^{ts}*, and *UAS-lacZ-RNAi* were characterized in previous studies (Kashio et al., 2016). *QUAS-mCD8-GFP* (#30002, #30003), and *v^{36f}* (#142) were obtained from the Bloomington *Drosophila* Stock Center. *UAS-v-RNAi 1* (v3349), *UAS-v-RNAi 2* (v107798), *UAS-cn-RNAi 1* (v105854), *UAS-cn-RNAi 2* (v11322), *UAS-kyat-RNAi 1* (v108093), *UAS-kyat-RNAi 2* (v22321), *UAS-kyat-RNAi 3* (v22322), and *UAS-sams-RNAi 1* (v103143) were obtained from the VDRC stock center.

Genotype Details

Fig. 1B

+/UAS-DtA^{ts}

WP-Gal4/UAS-DtA^{ts}

Fig. 1C

+/+;;WP-Gal4/UAS-DtA^{ts}

v^{36f}/ v^{36f};;WP-Gal4/UAS-DtA^{ts}

Fig. 2A-H

FB-Gal4/UAS-lacZ-RNAi;WP-QF2, QUAS-mCD8-GFP/+

FB-Gal4/+;WP-QF2, QUAS-mCD8-GFP/UAS-v-RNAi 1

FB-Gal4/UAS-v-RNAi 2;WP-QF2, QUAS-mCD8-GFP/+

FB-Gal4, QUAS-DtA^{ts}/UAS-lacZ-RNAi;WP-QF2, QUAS-mCD8-GFP/+

FB-Gal4, QUAS-DtA^{ts}/+;WP-QF2, QUAS-mCD8-GFP/UAS-v-RNAi 1

FB-Gal4, QUAS-DtA^{ts}/UAS-v-RNAi 2;WP-QF2, QUAS-mCD8-GFP/+

Fig. 3A

FB-Gal4/UAS-lacZ-RNAi;WP-QF2, QUAS-mCD8-GFP/+

FB-Gal4/+;WP-QF2, QUAS-mCD8-GFP/UAS-v-RNAi 1

FB-Gal4, QUAS-DtA^{ts}/UAS-lacZ-RNAi;WP-QF2, QUAS-mCD8-GFP/+

FB-Gal4, QUAS-DtA^{ts}/+;WP-QF2, QUAS-mCD8-GFP/UAS-v-RNAi 1

Fig. 3B, C

FB-Gal4, QUAS-DtA^{ts}/UAS-lacZ-RNAi;WP-QF2, QUAS-mCD8-GFP/+

FB-Gal4, QUAS-DtA^{ts}/UAS-cn-RNAi 1;WP-QF2, QUAS-mCD8-GFP/+

FB-Gal4, QUAS-DtA^{ts}/UAS-cn-RNAi 2;WP-QF2, QUAS-mCD8-GFP/+

FB-Gal4, QUAS-DtA^{ts}/UAS-kyat-RNAi 1;WP-QF2, QUAS-mCD8-GFP/+

FB-Gal4, QUAS-DtA^{ts}/UAS-kyat-RNAi 2;WP-QF2, QUAS-mCD8-GFP/+

FB-Gal4, QUAS-DtA^{ts}/UAS-kyat-RNAi 3;WP-QF2, QUAS-mCD8-GFP/+

Fig. 4B, D, F, H

FB-Gal4, QUAS-DtA^{ts}/+;WP-QF2, QUAS-mCD8-GFP/UAS-v-RNAi 1

Fig. 4C, E, G, H

FB-Gal4, QUAS-DtA^{ts}/UAS-lacZ-RNAi;WP-QF2, QUAS-mCD8-GFP/+

Fig. 5A

FB-Gal4, QUAS-DtA^{ts}/UAS-lacZ-RNAi;WP-QF2, QUAS-mCD8-GFP/+

FB-Gal4, QUAS-DtA^{ts}/+;WP-QF2, QUAS-mCD8-GFP/UAS-v-RNAi 1

FB-Gal4, QUAS-DtA^{ts}/UAS-sams-RNAi;WP-QF2, QUAS-mCD8-GFP/+

Fig. S1

+/UAS-DtA^{ts}

WP-Gal4/UAS-DtA^{ts}

Fig. S2A-E

FB-Gal4/UAS-lacZ-RNAi;WP-QF2, QUAS-mCD8-GFP/+

FB-Gal4, QUAS-DtA^{ts}/UAS-lacZ-RNAi;WP-QF2, QUAS-mCD8-GFP/+

Fig. S2F

w^{1118}

Fig. S3B,C

FB-Gal4, QUAS-DtA^{ts}/+;WP-QF2, QUAS-mCD8-GFP/+

Fig. S3D

UAS-lacZ-RNAi/+; WP-Gal4/+

WP-Gal4/UAS-v-RNAi 1

UAS-v-RNAi 2/+; WP-Gal4/+

UAS-cn-RNAi 1/+; WP-Gal4/+

UAS-cn-RNAi 2/+; WP-Gal4/+

UAS-kyat-RNAi 1/+; WP-Gal4/+

UAS-lacZ-RNAi 2/+; WP-Gal4,UAS-DtA^{ts}/+

WP-Gal4,UAS-DtA^{ts}/UAS-v-RNAi 1

UAS-v-RNAi 2/+; WP-Gal4,UAS-DtA^{ts}/+

UAS-cn-RNAi 1/+; WP-Gal4,UAS-DtA^{ts}/+

UAS-cn-RNAi 2/+; WP-Gal4,UAS-DtA^{ts}/+

UAS-kyat-RNAi 1/+; WP-Gal4,UAS-DtA^{ts}/+

Fig. S4A-D

FB-Gal4, QUAS-DtA^{ts}/UAS-lacZ-RNAi;WP-QF2, QUAS-mCD8-GFP/+

FB-Gal4, QUAS-DtA^{ts}/+;WP-QF2, QUAS-mCD8-GFP/UAS-v-RNAi 1

Fig. S5A

FB-Gal4/UAS-lacZ-RNAi;WP-QF2, QUAS-mCD8-GFP/+

FB-Gal4/+;WP-QF2, QUAS-mCD8-GFP/UAS-v-RNAi 1

FB-Gal4/UAS-v-RNAi 2;WP-QF2, QUAS-mCD8-GFP/+

FB-Gal4, QUAS-DtA^{ts}/UAS-lacZ-RNAi;WP-QF2, QUAS-mCD8-GFP/+

FB-Gal4, QUAS-DtA^{ts}/+;WP-QF2, QUAS-mCD8-GFP/UAS-v-RNAi 1

FB-Gal4, QUAS-DtA^{ts}/UAS-v-RNAi 2;WP-QF2, QUAS-mCD8-GFP/+

Fig. S5B

FB-Gal4, QUAS-DtA^{ts}/UAS-lacZ-RNAi;WP-QF2, QUAS-mCD8-GFP/+

FB-Gal4, QUAS-DtA^{ts}/UAS-cn-RNAi 1;WP-QF2, QUAS-mCD8-GFP/+

FB-Gal4, QUAS-DtA^{ts}/UAS-cn-RNAi 2;WP-QF2, QUAS-mCD8-GFP/+

FB-Gal4, QUAS-DtA^{ts}/UAS-kyat-RNAi 1;WP-QF2, QUAS-mCD8-GFP/+

FB-Gal4, QUAS-DtA^{ts}/UAS-kyat-RNAi 2;WP-QF2, QUAS-mCD8-GFP/+

FB-Gal4, QUAS-DtA^{ts}/UAS-kyat-RNAi 3;WP-QF2, QUAS-mCD8-GFP/+

Fig. S5C,D

UAS-lacZ-RNAi/+; WP-Gal4/+

WP-Gal4/UAS-v-RNAi 1

UAS-v-RNAi 2/+; WP-Gal4/+

UAS-cn-RNAi 1/+; WP-Gal4/+

UAS-cn-RNAi 2/+; WP-Gal4/+

UAS-kyat-RNAi 1/+; WP-Gal4/+

UAS-lacZ-RNAi 2/+; WP-Gal4,UAS-DtA^{ts}/+

WP-Gal4,UAS-DtA^{ts}/UAS-v-RNAi 1

UAS-v-RNAi 2/+; WP-Gal4,UAS-DtA^{ts}/+

UAS-cn-RNAi 1/+; WP-Gal4,UAS-DtA^{ts}/+

UAS-cn-RNAi 2/+; WP-Gal4,UAS-DtA^{ts}/+

UAS-kyat-RNAi 1/+; WP-Gal4,UAS-DtA^{ts}/+

Fig. S5E

FB-Gal4, QUAS-DtA^{ts}/+;WP-QF2, QUAS-mCD8-GFP/UAS-v-RNAi 1

Fig. S5F

FB-Gal4, QUAS-DtA^{ts}/UAS-lacZ-RNAi;WP-QF2, QUAS-mCD8-GFP/+

METHOD DETAILS

Temperature Shift Protocol for Temporal Cell Ablation

Embryos were laid at 25 °C for 4 h, and then shifted to 29 °C, 24 h after egg laying started. We defined this time point at after larval hatch (ALH) as 0 h. For ablation with $WP^{Gal4}>DtA^{ts}$, the temperature was raised to 29 °C for 48 h, and shifted to 18 °C from the early third instar larval stage. After maintaining an 18 °C temperature for 54 h, the temperature was returned to 29 °C and the flies were either allowed to pupate and eclose, or were dissected at the time points indicated during the BA and AA periods. For ablation with $WP^{QF}>DtA^{ts}$, the temperature was raised to 29 °C for 54 h from ALH 0 h, and shifted to 18 °C for 38 h. The temperature was returned to 29 °C after temporal ablation. Since we used a genetic cell ablation system, it took 38 h or 54 h to complete cell ablation. During this treatment, significant developmental delay should occur in cell ablation treatment. Thus, AA0 and AA6 between control and ablation are not the same developmental stage.

Wing Size Assessment

Flies were preserved in a mixture of ethanol/glycerin (3:1). Adult wings were mounted in Fluoromount-G™ (SouthernBiotech) after dissection in PBS. Images were captured with a Leica microscope DC 300 FX. We observed wing phenotypes by microscopy and manually classified the wing size into four categories: intact wings, group A; chipped or crumpled wings, group B; wings having a size <30% of control, group D; and wings with phenotypes intermediate between groups B and D, group C.

Immunohistochemistry

Discs were dissected in PBS and fixed with a 4% paraformaldehyde PBS solution, and washed with a 0.1% Triton X-100 PBS solution (PBST). Antibodies and dilutions used were: rabbit anti-cleaved Dcp1 (Asp216) 1:500 (Cell Signaling, 9578S), mouse anti-Wg (4D4) 1:500 (Developmental Studies Hybridoma Bank), rat anti-GFP (GF090R) 1:500 (NACALAI TESQUE, 04404-26), and rabbit anti-PH3 (Ser10) 1:3000 (Millipore, 06-570). Secondary antibodies used were: Alexa-Fluor antibodies (Life Technologies, A-21208, A-31571) and AffiniPure antibodies (Jackson Immuno Research, 712-165-153), diluted at 1:500. Probes used were: Hoechst 33342 (H3570) and Rhodamine Phalloidin (R415), diluted at 1:500 (Life technologies). Confocal images were taken with a Leica SP8 microscope. Number of repeated experiments were 2-3 in each experiment. Quantification of PH3 positive cells in WP region was performed with ImageJ.

Metabolome analysis using CE-TOF-MS

Two samples of 20 larval hemolymphs were collected at each indicated time point, and the cuticle was ruptured in cooled Milli-Q. The diluted hemolymph solution was then centrifuged at 300 ×*g*,

4 °C for 5 minutes. The collected supernatant was immediately frozen and kept at -80 °C. An internal standard solution 1 provided by HMT (Human Metabolome Technologies Inc., Yamagata, Japan) was freshly diluted with acetonitrile at each experiment according to the manufacturer's instructions. The centrifugal filter units 5K (ULTRAFREE MC PLHCC, HMT) were prewashed using Milli-Q water. Prepared acetonitrile was added to the collected supernatant and centrifuged at 2,300 ×*g*, 4 °C for 5 minutes. The supernatant was transferred to prewashed centrifugal filter units and centrifuged at 9100 ×*g*, 4 °C for 2 h. The sample tubes were evaporated with the centrifugal concentrator CC-105 (TOMY) at 1,400 rpm, at room temperature for 2-3 hours. The sample tubes were then kept at -80 °C until transport to the HMT. Targeted quantitative analysis of metabolites was performed by HMT, using capillary electrophoresis time of flight mass spectrometry (CE-TOF-MS). Transported larval hemolymph (two Control samples and two Ablation samples) were measured using CE-TOF-MS cation mode and anion mode. HMT metabolome library and Known-Unknown peak library were referred to for analysis. Then, 192 (102 cation and 90 anion) peaks were detected.

Metabolites extraction from larval samples

For the extraction of metabolites from the larval hemolymph, 5-10 or 20 larvae were collected at the indicated time points, and the cuticle was ruptured in cooled PBS. The diluted solution was then centrifuged at 1,000 ×*g*, 4 °C for 5 minutes. The collected supernatant was immediately frozen and kept at -80 °C. Methanol and chloroform were added to the samples and shacked. Samples were centrifuged at 2,300 ×*g*, 4 °C for 5 minutes. The centrifugal filter (Nanosep with 10K Omega, Pall Corporation) was prewashed with Milli-Q water. The supernatant was collected and transferred to a prewashed centrifugal filter unit and centrifuged at 14,000 ×*g*, 4 °C for 10-30 minutes. The content of the sample tubes was evaporated using the centrifugal concentrator CC-105 (TOMY). The pellet was diluted with Milli-Q water. The sample tubes were then kept at -80 °C until analysis. For the extraction of metabolites from the whole body or tissue samples, metabolites were extracted in 50% methanol from 5 whole larvae and 5-10 larval fat body, gut, cuticle, or brain. Samples were deproteinized using 50% acetonitrile and evaporated completely. The pellets were dissolved in Milli-Q water, followed by filtration using a 0.22 μm polyvinylidene fluoride (PVDF) filter (Millipore). The amount of proteins was quantified for normalization. Protein was extracted from the precipitates after metabolite extraction. The precipitates were washed in acetone and the protein was extracted with 0.1 N NaOH at 95 °C for 5 min. The amount of proteins was measured using a BCA Protein Assay kit (Thermo Scientific).

UPLC-MS/MS

Measurement of Trp, Kyn, 3-HK, and KynA was performed using ultra-high-performance liquid

chromatography equipped with tandem mass spectrometry, TQD (UPLC-MS/MS). In this study, we used UPLC-MS/MS of Waters or SHIMAZU. For the metabolite analysis by UPLC-MS/MS of Waters, extracted samples were diluted in an equal volume of 50 mM Tris-HCl (pH 8.8) with 100 μM dithiothreitol (DTT). For the metabolite analysis using UPLC-MS/MS of SHIMAZU, extracted samples were diluted in an equal volume of Milli-Q water. Each sample was injected, and the concentration was calculated based on the standard curve obtained from the serial dilution of the standard solution for each metabolite. Statistical analyses were conducted using GraphPad Prism software.

Quantitative RT-PCR

For quantitative RT-PCR (qRT-PCR), the total RNA was extracted from 5 larval fat bodies using the RNeasy Lipid Tissue Mini Kit and RNeasy Plus Mini Kit (QIAGEN). Total RNA (100 ng) was subjected to DNase digestion, followed by reverse transcription using the Takara PrimeScript RT Reagent Kit with gDNA Eraser. Quantitative PCR was performed using the Takara Premix Ex Taq II (Tli RNaseH Plus) and the Light Cycler 480 system (Roche). *RNA polII* was used as an internal control. Primer information is described as follows: *vermilion*: Forward primer, 5'-tggatgcccagtgtatgc; Reverse prime, 5'-tgcttgaaccaaagctcgta; *RNA pol II*: Forward primer, 5'-ccttcaggagtacggctatcatct; Reverse prime, 5'-ccaggaagacctgagcattaatct. Error bars represent the SEM, and p-values were calculated using a one-way analysis of variance (ANOVA) Tukey's multiple comparison test in GraphPad Prism software.

Feeding Experiments

TDO inhibitor (680C91) (SIGMA-ALDRICH) was diluted with dimethyl sulfoxide (DMSO) and 10 mM stocks were kept at -80 °C. Twenty microliters of 10 mM TDO inhibitor were added to 2 mL of fly food (4% cornmeal, 4% baker's yeast (Oriental Yeast), 10% glucose, 0.8% agar, propionic acid, and nipagin), and 100 μM TDO inhibitor food was prepared. Larvae transited to the 100 μM TDO inhibitor food 18 h before DtA^{ts} ablation stopped (AA-18) and 6 h after ablation (AA6). Kynurenic acid (SIGMA-ALDRICH) was diluted with 0.1 N NaOH and 20 mM stocks were kept at -80 °C. A volume of 50 μL or 100 μL of 20 mM stocks was added to 2 mL of fly food to make 0.5 or 1 mM KynA food. Larvae were transferred to KynA food at 0 h after ablation (AA0). As for the Wg phenotype, we classified it into three categories: DV boundary and inner ring of Wg were clearly observed, Class A; the Wg signal of DV boundary was scarce compared to inner ring of Wg, Class B; and hard to distinguish DV boundary and ring patterning of Wg, Class C.

QUANTIFICATION AND STATISTICAL ANALYSIS

The groups were compared using a one-way analysis of variance (ANOVA) Tukey's multiple

comparison test for Figure 1B, 3A, 5A, and S2A-F. For Figure 4B, 4C, S3C, an unpaired two-tailed Student's t-test was performed. The Chi-squared test was applied for Figure 1C, 2A, 3C, 4D, 4E, and S3D. Analyses were conducted using GraphPad Prism 6 (GraphPad Software, Inc., CA, USA). All error bars in the figures represent standard errors of the mean (SEM). No statistical methods were used to set the sample size. Experiments were neither randomized nor analyzed blindly.

SUPPLEMENTAL REFERENCES

Grönke, S., Beller, M., Fellert, S., Ramakrishnan, H., Jäckle, H., and Kühnlein, R.P. (2003). Control of fat storage by a Drosophila PAT domain protein. Curr. Biol. *13*, 603-606.

Kashio, S., Obata, F., Zhang, L., Katsuyama, T., Chihara, T., and Miura, M. (2016). Tissue nonautonomous effects of fat body methionine metabolism on imaginal disc repair in *Drosophila*. Proc. Natl. Acad. Sci. *113*, 1835-1840.

Kennerdell, J.R., and Carthew, R.W. (2000). Heritable gene silencing in Drosophila using double-stranded RNA. Nat. Biotechnol. *18*, 896-898.

Obata, F., Kuranaga, E., Tomioka, K., Ming, M., Takeishi, A., Chen, C.H., Soga, T., and Miura, M. (2014). Necrosis-driven systemic immune response alters SAM metabolism through the FOXO-GNMT axis. Cell Rep. *7*, 821–833.